ELSEVIER

Polymer 42 (2001) 6221–6230

polymer

www.elsevier.nl/locate/polymer

Modelling and simulation of the permanganic etching of banded spherulitic polyethylene: correlation with AFM observations

L. Markey, J.J. Janimak[1], G.C. Stevens*

Polymer Research Centre, School of Physics and Chemistry, University of Surrey, Guildford, Surrey GU2 7XH, UK

Received 20 October 2000; received in revised form 1 January 2001; accepted 22 January 2001

Abstract

Atomic force microscopy (AFM) has been used to examine the 3D profile of some permanganically etched metallocene catalysed high-density polyethylenes. Banded spherulites were observed with an asymmetric band radial profile, having a characteristic shape with specific 'inner' and 'outer' band slopes, the inner slope being much lower than the outer slope. Permanganic etching is known to produce surface etching that is more rapid for the amorphous part of the polymer than for the crystalline part. A mathematical model of the etching process was developed to demonstrate that band asymmetry can stem from differential etching and to fully simulate the entire resultant relief. Etching was modelled analytically in a 3D geometry, based on the scalar product of two etch vectors, the first of which, **c**, is locally perpendicular to the lamella and secondly **p**, locally perpendicular to the specimen surface. By modelling a banded spherulite with vector **c** constantly perpendicular to the spherulite radius and having its extremity following a helical trajectory, it is possible to calculate the scalar product **c**·**p** at any point on the surface. This product gives a formula capable of calculating etch profile development as a function of time and for any initial surface profile, with the following parameters: etching rates of groups of flat-on lamellae and groups of edge-on lamellae, interband spacing, distance of the spherulite centre from the initial surface. Simulations of the etching of banded spherulites were performed and the parameters adjusted to give a very food fit to many AFM observations. The model confirms that the observed AFM profile of banded spherulites in polyethylene is probably of geometric origin alone. It is shown that the observed slope asymmetry is not material dependant, i.e. molecular weight or other structural parameters. The model not only explains the slope asymmetry but also gives a good simulation of band height and its radial variation, etching depth and apparent band period. It could also be used to estimate the relative speed of the permanganic etching of different crystal facets and the amorphous phase. Further refinement of the modelling work on other semicrystalline polymers amenable to permanganic etching is also a possibility. © 2001 Elsevier Science Ltd. All rights reserved.

Keywords: Permanganic etching; Spherulites; Atomic force microscopy

1. Introduction

Permanganic etching was first developed for polyolefins in the late 1970s by Olley, Hodge and Bassett [1] and has been refined and extended over the years to include a much wider family of polymer materials [2–8]. Up and until then, techniques like nitric acid etching and chlorosulphonic acid staining were commonly used to monitor the development of lamellar structure via transmission electron microscopy (TEM) [9–12]. More recently, atomic force microscopy (AFM) has become more accessible enabling observations of detailed microstructure down to the nanoscopic level, in particular lamella resolution. To date only limited quantitative and kinetics studies of permanganic etching have been published by Naylor et al. in 1983 [13] and Freedman et al. in 1986 [14].

Polymer spherulites are an important morphological form in semi-crystalline polymers frequently observed using polarised light optical microscopy [15–21]. Spherulites are characterised by a radial crystal growth pattern that evolves into an object having spherical symmetry [22]. Banded spherulites have been unambiguously identified as exhibiting a regular arrangement of birefringent units rotating around the spherulite radius [10,15–21]. Under isothermal crystallization conditions, the appearance of a constant helical pattern is inferred from conventional optical and electron microscopies without any direct measure of band profile. These observations have also led to acceptance that many systems exhibit regular band period spacing. In other words every one half twist (π-rotation about the spherulite radius) corresponds to one band period spacing. However, it appears that the origin and observation of

* Corresponding author. Tel.: +44-0-1483-259599; fax: +44-0-1483-259555.

E-mail address: g.stevens@surrey.ac.uk (G.C. Stevens).

[1] Present Address: Lilly Clinical Operations SA. Parc Scientifique de Louvain-la-Neuve, Rue Granbonpré 11, 1348 Mont-Saint-Guibert, Belgium.

0032-3861/01/$ - see front matter © 2001 Elsevier Science Ltd. All rights reserved.
PII: S0032-3861(01)00097-0

banded spherulites is largely determined by choice of catalyst, molecular weight of the polymer and an appropriate nucleation and crystallization process, anyone of which may produce a dominant effect. In previous studies of medium density polyethylenes, we have found a wide range of morphologies extending from lamellae domaining through to fully developed banded spherulites whose band period is controlled by molecular characteristics and crystallization conditions [23]. Spherulites are essentially spherical aggregates of anisotropic crystalline lamellae that emanate from a common central nucleus. In a diametral section, the lamella crystallographic *b*-axis is radial, while *c* is near normal to the section for flat-on lamellae.

Observations of banded spherulites have been reported on polyethylene, as well as on many other polymeric or inorganic materials. Most TEM and AFM observations of polymeric banded spherulites reveal an apparent band period spacing which decreases from the centre of the spherulite and has a purely geometric explanation [24,25]. We have shown that the apparent radial decrease in band spacing obeyed a square root law of the distance from the centre of the spherulite, and occurs for all non-diametral sections of spherulites [25].

AFM imaging of permanganically etched sections of polymers has been extensively studied in recent years. The key advantages of using AFM over conventional TEM is its ability to add 3D vertical information and to image polymer surfaces directly without the need for heavy element staining and time-consuming two-stage replication [26]. This has also permitted direct imaging of the crystallisation of polymers [27–30].

In this paper, we attempt to reproduce the geometric origin of the AFM observations of the profile of etched surfaces. Using a simple 3D etching model, we not only simulate the observed band spacing decrease but also the shape of the whole profile, including band asymmetry, band height and its radial variation and etching depth.

2. Materials and specimen preparation

Medium and high density polyethylenes with known branch content, molecular weight and polydispersity were kindly provided by Fina Research (Belgium) and Solvay (Belgium) through the Fina Surrey Scholar research programme. All our polymers were metallocene catalysed. The characteristics of the polymers studied in this paper are detailed in Table 1.

Specimens were melt-crystallized under a dry nitrogen atmosphere at 170°C in a Linkam hot stage and subsequently cooled at 15°C/min down to room temperature. Specimens were then etched for 3 h in an etchant consisting of a 1% w/v solution of potassium permanganate dissolved in 2:1 sulphuric and dry ortho-phosphoric acids [14]. Periodic checks on the progress of etching were undertaken, by arresting the etching process and observing development with the optical microscope.

Table 1
Molecular and physical characteristics of as received material. Short chain branch content was assessed using C^{13} NMR

Reference	Polymer A	Polymer C	Polymer D
Resin type	Homopolymer	Homopolymer	Copolymer
Density (g/cm^3)	0.9602	0.9545	0.9508
M_n (kDa)	23.4	30.8	27.3
M_w (kDa)	79	118	100.4
M_z (kDa)	246	321	305
M_w/M_n	3.38	3.83	3.68
SCB (/1000C)[a]	0	0	0.2
T_m (°C)	133.9	131.8	134.1
ΔH_m[b](J/g)	220.4	217.1	212.9

[a] 1-Hexene comonomer.
[b] 100% Crystallinity (293 J/g).

3. Experimental AFM observations

Etched samples were observed directly using tapping mode AFM on a Digital Instrument Nanoscope III scanning probe microscope, using NT-MDT non-contact ultrasharp silicon cantilevers or DI 'nanosensors' tips. Experiments were conducted in the tapping mode, with the cantilever vibrating near its resonance frequency. Vertical *z*-axis cross-sections were taken as line profiles in the *x*–*y* plane from unmodified topographic images to reveal the surface profile of permanganically etched banded spherulites. Data were retrieved from the DI software in the form of ASCII files of *z*-data accompanied with values of *z*-sampling parameter and scale, along with the lateral size value. These data were then processed to produce real spatial information. Where specified, topographic images were processed for contrast enhancement using a standard DI programme, which runs a statistical differencing filter enhancing the contrast of edge and line features, enabling lamellar structure to be better revealed. This image treatment distorts the *z*-axis scale. This is why the *z*-axis height bar is not displayed next to the contrast-enhanced image (Fig. 2a) as it is not valid. These contrast-enhanced images were useful in providing features very similar to those observed in TEM, i.e. the details of lamellar orientation. Phase images have the same ability but they are not presented here to maintain clarity.

AFM imaging of a series of permanganically etched metallocene catalysed high-density polyethylenes (mHDPEs) reveals banded spherulites, as shown in Fig. 1a for Polymer C. Images of spherulitic polymers A and D are not presented here but can be seen elsewhere [25]. Highlighted in Fig. 1a is spherulite 1, which is subsequently used later in the simulation study. A zoomed image of spherulite 1 is presented in Fig. 1b and this is also used later to obtain a higher resolution of the profile. Fig. 2a is the contrast-enhanced counterpart of

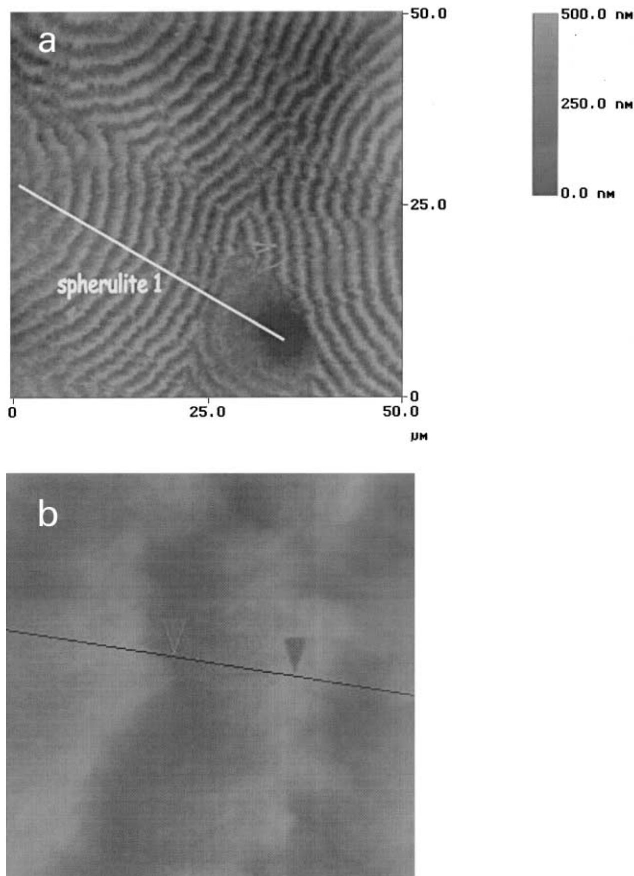

Fig. 1. (a) 50×50 μm AFM ('tapping') height image of etched spherulitic polymer C. (b) 5×5 μm zoom of spherulite 1.

Fig. 1b, while Fig. 2b presents the cross-section of the image of Fig. 1b in a vertical x–z plane (i.e. perpendicular to the specimen's surface) along the black line shown in Fig. 1b. We define the inner and outer band slopes as the ascending and descending slopes in the profile where the x-axis starts from the centre of the spherulite. An asymmetric profile characterised by different values of the inner and outer band slopes is observed. In the examples presented here, they were typically of the order of 15° and −55°, respectively. This observation adds to the already reported decrease in the apparent band period from the centre of the spherulite, which was explained by a simple geometrical argument in earlier work [24,25].

Fig. 2a shows the variations in orientation of the lamellae at different radial positions. The edges of stacked lamella ('edge-on') can be observed in the valley regions of the bands, while 'flat-on' lamellae are at the top of the bands. As observed in Fig. 2b, lamellar relief results in small oscillations in the line profile, which can be seen in the AFM contrast enhanced images (or using the phase signal without image processing). The model developed below cannot simulate these local protrusions (at nanometer-level). Instead, it monitors the overall shape of the bands and shows how this shape in intimately linked to lamellar orientation.

4. Geometric model of permanganic etching

Permanganic etching of polyethylene relies on differential surface dissolution with a speed that is dependent on the material present at the surface. Dissolution is especially active in the amorphous regions compared to the crystalline regions (the lamellae) where the process is measurably slower. Furthermore, as lamella crystals are anisotropic,

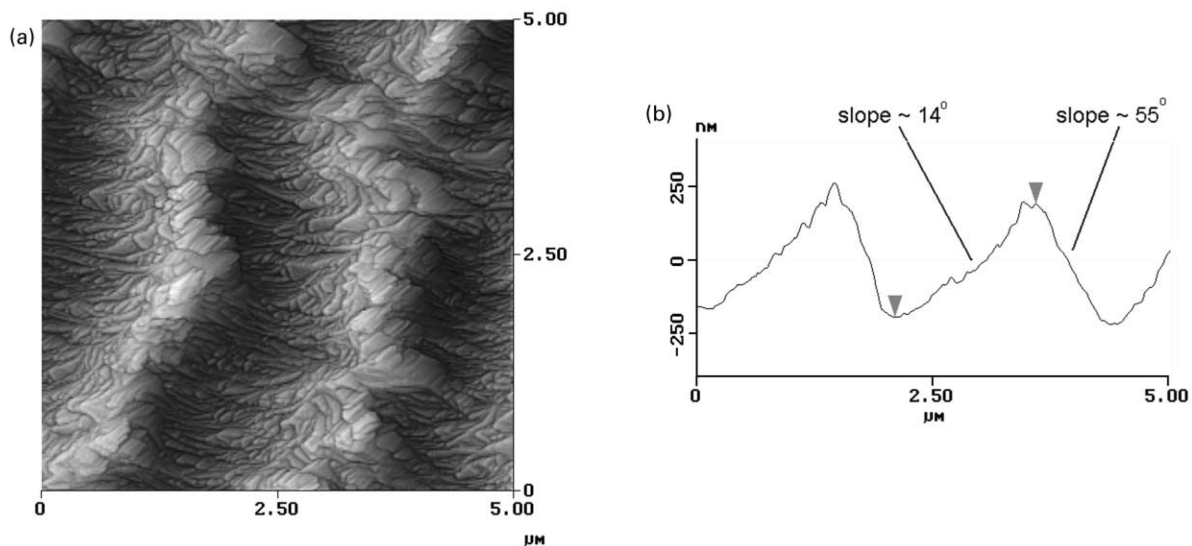

Fig. 2. (a) 5×5 μm AFM (tapping) contrast-enhanced image of etched Polymer C (counterpart to Fig. 1a). Vertical scale is not represented because of distortion in the z-axis; similar image is obtained in phase mode image. (b) cross-section of spherulite 1 along the line shown in Fig. 1b.

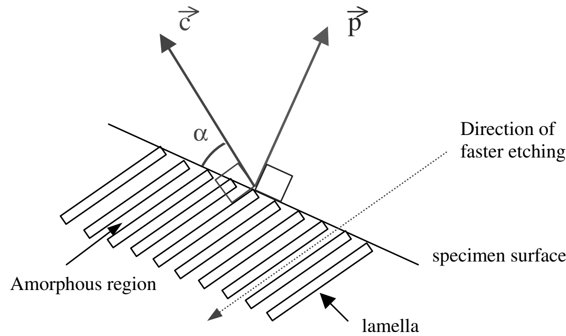

Fig. 3. Local positions for vectors **c** and **p** with respect to lamella and surface orientation.

stacked lamellae are etched preferentially in the direction parallel to the lamellar planes. A maximum etch rate is reached in that direction, whereas the minimum etch rate is obtained in the perpendicular direction (see Fig. 3). The corresponding extremes of the etching speed will be referred to as m and k, respectively, in the following. We believe that the reason for this difference between the etching rates in regions with flat-on lamellae and regions with edge-on lamellae lies in the faster penetration of the etchant into the amorphous regions and the easier dissolution of polymer chains at lamella edges. As mentioned earlier, the purpose of this paper is not to explain the etching mechanism itself, but rather to show that the geometric shape of the profile is consistent with a differential etch-rate mechanism.

The surface etching profile is determined by the distribution envelope of surface edges of the lamellae, as depicted in Fig. 3. We have developed a geometrical etching model that is based on the calculation of the vector perpendicular to the lamella basal plane, called vector $\vec{c}$. The 3D directional variations of $\vec{c}$ depend on the type of polymer microstructure. In a non-spherulitic material consisting of domains of locally ordered lamellae, $\vec{c}$ does have an order locally in each domain (at the mesoscopic level), but is random overall on a larger scale. In contrast, spherulitic materials with spherulite sizes reaching several tens of μm have longer range order.

For any point M sitting on the surface, let us consider the angle α between the surface of the specimen and $\vec{c}(M)$, the unity vector locally perpendicular to the lamella. Also, let us consider the vector $\vec{p}(M)$ normal to the surface of the specimen and normalised to unity. We assume that the etching rate gradient $E(M)$ can be written as follows:

$$E(M) = k + (m - k)(\cos \alpha(M))^2, \tag{1}$$

where k and m are positive constants and $k < m$. Note that M will be omitted in the following.

If a group of lamella is flat-on, we have $\alpha = 90°$, then $E = k$, the minimum value E can take. If the lamellae are edge-on, we have $\alpha = 0°$, then $E = m$, the maximum value E can take. Therefore k and m can be defined as the etching rates of a stack of flat-on lamellae or a stack of edge-on lamellae, respectively. As these etching rates take into account the contributions of both crystalline (lamellae) and amorphous phases, they cannot be assimilated to the etching rates of a single lamella. Finally, no evolution of the chemical characteristics of the system during etching is taken into account, therefore no reaction product build-up on the surface is considered which might impede further etching, as was reported by Naylor et al. [13].

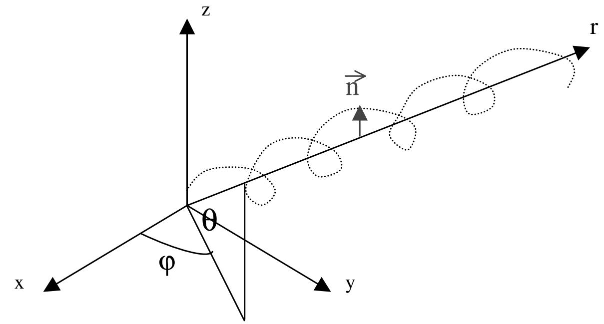

Fig. 4. Trajectory of vector **c** in a banded spherulite centred at the origin.

Let us introduce the scalar product of $\vec{c}$ and $\vec{p}$ (vectors normalised to 1):

$$\vec{c}\cdot\vec{p} = \|\vec{c}\|\cdot\|\vec{p}\|\cos(\pi/2 - \alpha) = \sin \alpha \tag{2}$$

and using

$$\cos^2 \alpha = 1 - \sin^2 \alpha = 1 - (\vec{c}\cdot\vec{p})^2. \tag{3}$$

Then:

$$E = k + (m - k)[1 - (\vec{c}\cdot\vec{p})^2]. \tag{4}$$

This general equation giving the etching rate at any point of the surface is valid, potentially, for any lamellar material, provided the vector field **c** is known for this material. In the following we calculate the analytical expressions of **c** and **p** at any point in the Cartesian coordinates (x,y,z) for the system studied.

4.1. Spherulite modelling (calculation of vector field **c***)*

Let us consider a spherulite with an interband distance d and its centre positioned at the origin. We model an ideal banded spherulite by the vector $\vec{c}$, constantly perpendicular to the spherulite radius and having its extremity following a regular helical trajectory. However, this ideal description is true only away from the nucleus; at the nucleus, not all the lamella are parallel to the spherulite radius. The following expressions of $\vec{c}$ are therefore only valid at radial distances greater than a certain unknown distance d_{nucleus} which is assumed to be smaller than d in the simulation developed later. Let us write $\vec{c}$ in the spherical coordinates as (r,θ,φ). Thus, for an ideal spherulite, $\vec{c}$ has no radial component (r-axis) and rotates around the r-axis as a function of r with an angle of rotation ω proportional to r (see Fig. 4). Thus $\vec{c}$ is

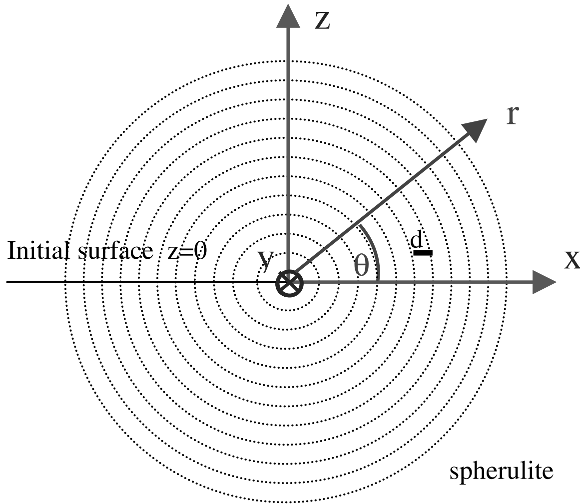

Fig. 5. Simplified situation in the x–z plane considered in the calculations.

only a function of r and d, and could be represented by:

$$\vec{c}_{r,\theta,\varphi} = \begin{pmatrix} 0 \\ \cos\omega \\ \sin\omega \end{pmatrix} \qquad \text{with } \omega = \frac{\pi r}{d} \tag{5}$$

with $\vec{c}$ normalised to 1 ($\|\vec{c}\| = 1$, meaning that $c_r^2 + c_\theta^2 + c_\varphi^2 = 1$).

We now have to relate the variable change of (r,θ,φ) into Cartesian coordinates (x, y, z). To simplify the problem, we take $\varphi = 0$, so that $y = 0$ and everything takes place in a vertical plane, i.e. perpendicular to the initial surface of the specimen. This simplification is valid because of the spherical symmetry of the system away from the nucleus as shown in Fig. 5.

In this configuration,

$$\vec{c}_{r,\theta,\varphi} = \begin{pmatrix} c_r \\ c_\theta \\ c_\varphi \end{pmatrix}$$

is transformed into

$$\vec{c}_{x,y,z} = \begin{pmatrix} c_x \\ c_y \\ c_z \end{pmatrix}$$

by the operations:

$$\begin{cases} c_x = c_r\cos\theta - c_\theta\sin\theta \\ c_y = c_\varphi \\ c_z = c_r\sin\theta + c_\theta\cos\theta \end{cases}$$

resulting in $\vec{c}_{x,y,z} = \begin{pmatrix} -\sin\theta\ \cos\omega \\ \sin\omega \\ \cos\theta\cos\omega \end{pmatrix}$. (6)

The coordinate change implies $x = r\cos\theta$, $z = r\sin\theta$ and $r^2 = x^2 + y^2$.

Thus

$$\vec{c}_{x,y,z} = \begin{pmatrix} -\dfrac{z}{r}\cos\omega \\ \sin\omega \\ \dfrac{x}{r}\cos\omega \end{pmatrix} = \begin{pmatrix} \left(z/\sqrt{x^2+z^2}\right)\cos\left(\dfrac{\pi}{d}\sqrt{x^2+z^2}\right) \\ \sin\left(\dfrac{\pi}{d}\sqrt{x^2+z^2}\right) \\ \left(x/\sqrt{x^2+z^2}\right)\cos\left(\dfrac{\pi}{d}\sqrt{x^2+z^2}\right) \end{pmatrix}. \tag{7}$$

The above Eq. (7) is only true for a spherulite centre situated on the surface. If the centre of the spherulite lies at a distance 'a' beneath the surface (on the z axis), then z must be replaced by $(z + a)$ in the above equation.

4.2. Expression of vector p

Let us now calculate vector $\vec{p}$, which is constantly perpendicular to the etched surface. This takes place with the geometric simplification $\varphi = 0$, implying that $y = 0$. As vector $\vec{p}$ is always in the (r, θ) plane, the simplification implies that $\vec{p}$ is always in the (x, z) plane too ($p_y = 0$).

$$\vec{p}_{x,y,z}(x,t) = \begin{pmatrix} p_x \\ 0 \\ p_z \end{pmatrix} \qquad \text{with } \|\vec{p}\| = p_x^2 + p_z^2.$$

The initial situation (time $t = 0$) before the etching starts is supposed to be a flat specimen surface defined by the equation $z = 0$. As we have eliminated the y coordinate and are working in the (x, z) plane, the surface is now only defined by its z profile, which is a function of x and t. The notation $H(x, t)$ defines this resulting profile. Introducing the surface in the system breaks the spherical symmetry, however the system remains symmetric with respect to the z-axis.

At $t = 0$, $H(x) = 0$ (flat profile). At any t, we have the situation described in Fig. 6. In order to find the expression of $\vec{p}(x, t)$ we can consider finding first the expression for the

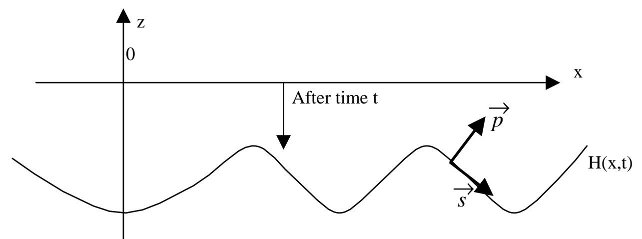

Fig. 6. Etched specimen surface at time t. Position of vectors $\vec{p}$ and $\vec{s}$.

position vector $\vec{s}_{x,z}(x,t) = \begin{pmatrix} s_x \\ s_z \end{pmatrix}$, which is the unity vector tangential to $H(x,t)$.

We have $\dfrac{s_z}{s_x} = \dfrac{dH}{dx}$ and $s_x^2 + s_z^2 = 1$.Thus

$$\vec{s}_{x,z}(x,t) = \begin{pmatrix} \dfrac{1}{\sqrt{1+(dH/dx)^2}} \\ \dfrac{dH/dx}{\sqrt{1+(dH/dx)^2}} \end{pmatrix}. \tag{8}$$

To find $\vec{p}(x,t)$, we can apply a multiplication with the $\pi/2$ rotation matrix:

$$\begin{pmatrix} p_x \\ p_z \end{pmatrix} = \begin{pmatrix} 0 & -1 \\ 1 & 0 \end{pmatrix} \begin{pmatrix} s_x \\ s_z \end{pmatrix}. \tag{9}$$

Hence

$$\vec{p}_{x,z}(x,t) = \begin{pmatrix} -\dfrac{dH/dx}{\sqrt{1+(dH/dx)^2}} \\ \dfrac{1}{\sqrt{1+(dH/dx)^2}} \end{pmatrix}, \tag{10}$$

where $H(x,t)$ is the profile of the etched surface.

4.3. Modelling the etching of a spherulite

By replacing $\vec{c}$ and $\vec{p}$ by their analytical expressions in Eq. (4), we obtain:

$$\vec{c}\cdot\vec{p} = \begin{pmatrix} -\left((z+a)/\sqrt{x^2+(z+a)^2}\right)\cos\left(\dfrac{\pi}{d}\sqrt{x^2+(z+a)^2}\right) \\ \sin\left(\dfrac{\pi}{d}\sqrt{x^2+(z+a)^2}\right) \\ \left(x/\sqrt{x^2+(z+a)^2}\right)\cos\left(\dfrac{\pi}{d}\sqrt{x^2+(z+a)^2}\right) \end{pmatrix} \times \begin{pmatrix} -\dfrac{dH/dx}{\sqrt{1+(dH/dx)^2}} \\ 0 \\ \dfrac{1}{\sqrt{1+(dH/dx)^2}} \end{pmatrix}. \tag{11}$$

Therefore, the expression for the etching rate gradient $E(x,H(x))$ is:

$$E(x,H(x)) = k + (m-k) \times \left\{ 1 - \frac{[\cos((\pi/d)\sqrt{x^2+(H(x)+a)^2})]^2[(H(x)+a)(dH/dx)+x]^2}{(x^2+(H(x)+a)^2)(1+(dH/dx)^2)} \right\}. \tag{12}$$

The expression $[E(x,H(x))dt]$ represents the thickness of etched material removed during dt at coordinates $(x, H(x))$. E is the etching rate in the direction perpendicular to the surface, but as we actually need the etching rate in the vertical direction z for the simulation, we correct Eq. (12) for the angle β as indicated Fig. 7.

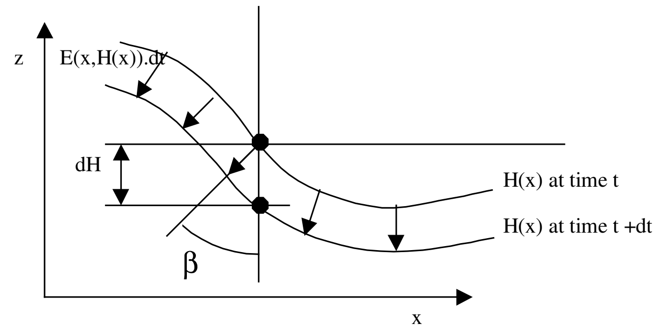

Fig. 7. Schematic showing the etching depth during a time interval dt.

By approximation, we have:

$$\cos\beta = \frac{E(x,H(x))dt}{dH(x)}. \tag{13}$$

Thus the z variation of the $H(x)$ profile after dt seconds (vertical etching depth) is:

$$\begin{aligned} dH(x) &= dtE(x,H(x))\left(\frac{1}{\cos\beta}\right) \\ &= dtE(x,H(x))\left(\frac{1}{\cos(\tan^{-1}(dH/dx))}\right). \end{aligned} \tag{14}$$

As $\cos a = 1/\sqrt{1+\tan^2 a}$ we have

$$\left(\frac{1}{\cos(\tan^{-1}(dH/dx))}\right) = \sqrt{1+\left(\frac{dH}{dx}\right)^2}. \tag{15}$$

Hence

$$dH(x) = dtE(x,H(x))\sqrt{1+\left(\frac{dH}{dx}\right)^2}. \tag{16}$$

Eqs. (12) and (16) provide dynamic analytical expressions of the etching profile away from the nucleus, as a function of the physical parameters (d: interband spacing, a: distance of the centre of the spherulite to the surface, k: etching rate of flat-on lamella stack, m: etching rate of edge-on lamella stack, dt: time interval). By carefully choosing these parameters and starting from a given initial profile $H_0(x, t=0)$ it is possible to calculate iteratively the surface's etched profile at any time by using these two equations.

5. Simulation method

Computer simulation of the etching of a banded spherulite according to the model was performed on a PC using Microsoft Excel and Visual Basic macros. The surface etched profile was calculated iteratively from a flat initial profile ($H_0(x, t=0) = 0$). The sampling frequency in the x direction was generally kept to 100 points per band period (i.e. x-interval $= d/100$). The dt interval was chosen at about 0.005 h (18 s). During preliminary simulation tests, we observed the appearance of some artefacts (oscillations) in

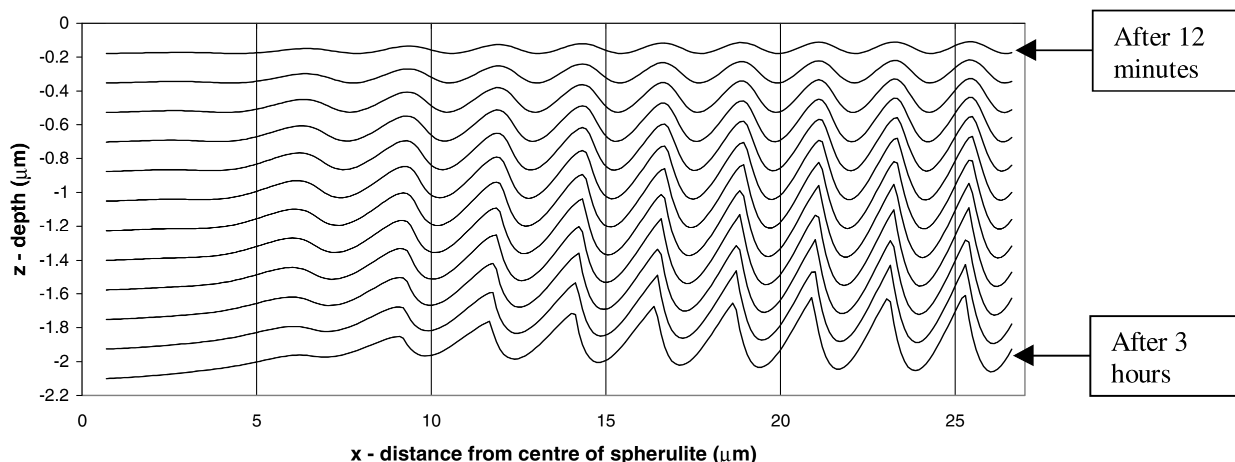

Fig. 8. Etching simulation of a spherulite over a 3 h period. Consecutive cross-sections represent 12 min time intervals. Simulation parameters were: $d = 2.05$ μm, $a = -8$ μm, $k = 0.4$ μm/h, $m = 0.65$ μm/h, d$t = 0.002$ h, x-interval $= d/100$ μm with a 5-point Savitsky-Golay smoothing every 100 iterations.

areas of high 'slope' occurring after several tens or hundreds of iterations depending on the parameters values. (The slope was defined as the derivative of the profile with respect to x.) This anomaly was due to chaotic divergence of the iterative calculation caused by the sampling interval being too large. However, instead of decreasing this interval, in order to keep calculation times short, we chose to introduce a smoothing operation of the profile every N iterations to remove the divergence before it became a problem. Also, we were careful not to modify the profile's shape too much with an N too low. Smoothing was performed following the Savitsky-Golay method [31–33] with either 5 or 9 points. 5-points smoothing was judged sufficient in most cases. In order not to modify the sharp tops of the bands, smoothing was performed by segment, each segment being defined by two consecutive band maxima.

In summary, two types of parameters enter into the fitting routine. Firstly material parameters, d, a, k and m and secondly, approximation parameters linked to the discrete aspect of the calculation method itself. These are dt, the time interval, s, the x-sampling interval between two points and N, the number of iteration prior to Savitsky-Golay smoothing.

Fig. 8 shows an example of a simulation for a non-diametral section through a spherulite. We can see the increase in depth and band height with increasing time, as well as the evolution towards a strong asymmetry in the shape of individual band profiles. Also, the lateral decrease in the apparent band spacing already reported in earlier work is readily simulated.

6. Fitting of AFM data and discussion

Results of simulations compared to experimental AFM data on one particular material (polymer C) is first presented as an example of the fitting process. The results obtained for the three polymers A,C and D are discussed at the end of this section. We have analysed the vertical cross-sections of the two images (untreated raw data) presented in Figs. 1a and b. The magnified 5×5 μm image of Fig. 1b was used to get a better resolution. Fits were adjusted manually, i.e. each of the simulation parameters were changed one at a time until the best fit was reached. For each fit, an x-offset was also applied to the experimental data set and adjusted to properly align experimental and fitted profiles but care was taken to keep the actual spherulite-centre abscissa and the fit centre abscissa coincident. The use of this x-offset is justified by the large uncertainty in the determination of the coordinates of the spherulite's centre, due to the divergence from ideality in the centre of the spherulite. These corrections are needed because of the use of single (not averaged) cross-sections, which contain local variations due to local protruding and receding lamellae and defects. For uniform spherulitic structures, this problem could be overcome by using averages of several radial cross-sections but here we have chosen to keep the original data, being careful to take cross-sections in regions containing as few irregularities as possible. In addition, in some cases, it was also necessary to apply a linear baseline correction in order to account for slope in the image.

Fig. 9 shows the best fit obtained on a cross-section of Fig. 1a (along the white line). The first parameters to be fixed were d and a. These two parameters are intimately linked as they determine together the radial variation of the interband distance. A true band period $d = 2.05$ μm was found and it was noticed that the quality of the fitting was very sensitive to this parameter. We thus think that thanks to this simulation method, a higher precision can be attained in the determination of the true band period. The distance 'a' of the centre of the spherulite from the initial surface was adjusted to an approximate value of -8 μm. This value is unique because this parameter results from the fitting of the interband distance variations along the r-axis. The quality of the fitting seems less sensitive to this parameter than it was for d but we believe that an accuracy

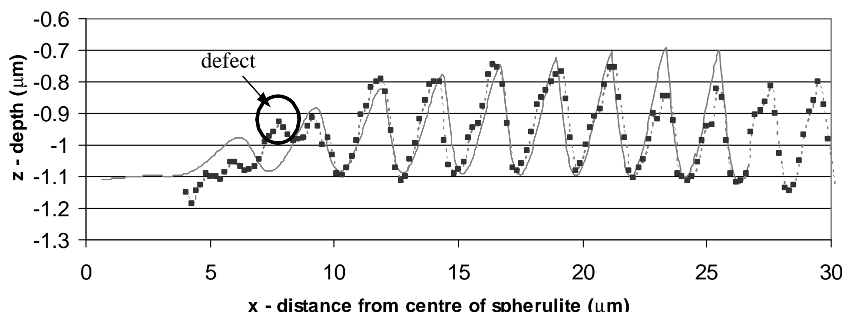

Fig. 9. Etched spherulite vertical cross-section (Polymer C): experimental AFM data as symbols (taken along line 1 indicated in Fig. 1a) compared with simulation (plain line) best fit obtained with parameters $d = 2.05$ µm, $a = -8$ µm, $k = 0.2$ µm/h, $m = 0.37$ µm/h, $dt = 0.003$ h, x-interval = $d/100$ µm, with a 5-point Savitsky-Golay smoothing every 100 iterations. Circled is a portion of the profile where a defect is present.

of ± 1 µm can be obtained on 'a'. Parameters k and m were set at 0.2 and 0.37 µm/h, respectively. Apart from the two extremities, the fits were good. The first misfit occurred below 8 µm on the x-axis and the other one above 23 µm. However, these misfits can be largely explained by the expected defects of the sample and the fact that the real initial surface is not perfectly flat. As can be seen on the AFM images, spherulites present some defects that could explain the hump observed between $x = 7$ and 8 µm. For the far right part of the profile, we probably have a discontinuity (at ~22 µm) in the initial surface profile. This hypothesis is supported by the observation that after this discontinuity, the band height starts increasing again, as can be expected in a re-established defect-free situation.

The fit of the zoomed image of Fig. 1b obtained with the same fitting parameters values as in Fig. 9 is displayed in Fig. 10. In order to take into account the discontinuity observed at ~24.4 µm, the simulation data was segmented into two, with the right part slightly shifted vertically by −0.02 µm. The fit is good and shows the difference between the inner and outer slopes (~15° and ~55° respectively). However, a better fit was obtained with different k and m parameters, as shown later in Fig. 11.

A better fit in the zoomed area was obtained with $k = 0.4$ µm/h and $m = 0.65$ µm/h (see Fig. 11), to be compared to 0.2 and 0.37 for the previous fit. The variance was approximately 12% lower than for the previous fit (note: the variance was calculated over two radial band periods). In addition, when looking very closely at the shape of the ascending parts of the two bands, it can be observed that the fitted line is straighter than the line of the previous fit, especially towards the top of the profile, which is more in accordance with the shape of the experimental profile. The band shape is nicely fitted, except in the lower part of the bands. We have observed that the band shape is dependent on the spherulite chosen for the analysis. Therefore, the observations reported here are not representative of all the spherulites. S-shaped ascending profiles were also observed in other cases. The important difference in the k and m values for the two images is not yet understood. Nevertheless, we have observed that in either case, the ratio k/m has to be kept roughly constant at around 0.6 to achieve good fits. Again, as in Fig. 10, the right segment of the simulation for the fit to Fig. 11 was slightly shifted vertically by −0.02 µm to account for the observed discontinuity.

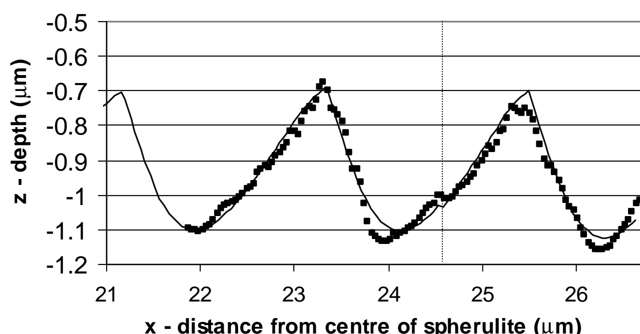

Fig. 10. Etched spherulite vertical cross-section across two bands (Polymer C): experimental AFM data as symbols, taken on the zoomed image of Fig. 1b, compared with simulation (plain line) obtained with the same parameters as in Fig. 9. The vertical dotted line indicates that simulation data has been segmented at that abscissa with the right segment slightly shifted vertically by −0.02 µm to take into account the discontinuity of the experimental data (see text).

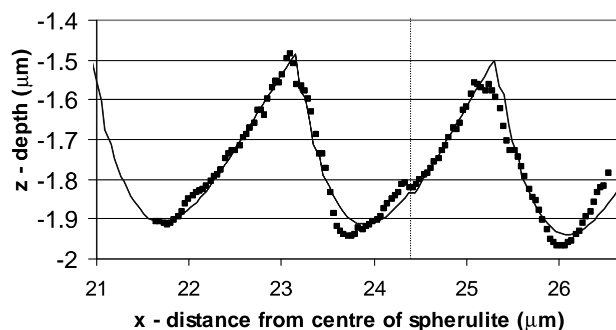

Fig. 11. Etched spherulite vertical cross-section across two bands (Polymer C): experimental AFM data as symbols, taken on the zoomed image of Fig. 1b, compared with the best fit (plain line). Best fit was obtained with the following parameters, $d = 2.05$ µm, $a = -8$ µm, $k = 0.4$ µm/h, $m = 0.65$ µm/h, $dt = 0.003$ h, x-interval = $d/100$ µm, with a 5-point Savitsky-Golay smoothing every 100 iterations. The vertical dotted line indicates that simulation data has been segmented at that abscissa with the right segment slightly shifted vertically by −0.02 µm to take into account the discontinuity of the experimental data (see text).

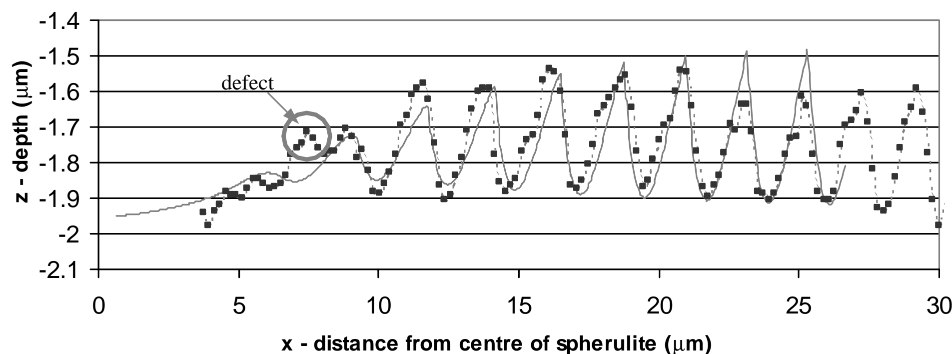

Fig. 12. Etched spherulite vertical cross-section (Polymer C): experimental AFM data as symbols (taken along the spherulite line 1 indicated in Fig. 1a compared with simulation (plain line) obtained with the same parameters as in Fig. 11. Circled is a portion of the profile where a defect is present.

The results of the fitting routine of the profile of the larger size image (Fig. 1a) with the parameters used in the last case (i.e. with the higher values of k and m) are presented in Fig. 12. We obtained a correct overall fit that was not as good as the first fit in Fig. 9, except in the left part of the profile ($x < 10$ µm). This can be explained by the poorer resolution of the large image, and by the multiplication of microstructural defects in the long range that inevitably produces more misfits.

The problem in the optimisation of the fitting due to the use of different values of k and m in the two images does not however reduce the overall quality of the simulation which validates the model. As fits were made on single cross-sections, they would probably benefit from comparison with averaged profiles from several different radial cross-sections, as already mentioned. An automated mathematical tool needs to be used to average several radial profiles of a spherulite

By studying polyethylene containing two populations of lamellae with different lamella thicknesses, Freedman et al estimated etching rates of 1.6 Å/s for the thinnest lamellae and 3.3 Å/s (or 1.8 Å/s after annealing) for the thickest ones [14], corresponding to 0.58 and to 1.19 or 0.65 µm/h, respectively. These values tend to favour the second fit ($k = 0.4$ µm/h and $m = 0.65$ µm/h), obtained from the zoomed image. Refinement of the model could be conducted in different ways. Estimation of k and m etching rates could be improved by introducing parameters such as the local crystallinity and lamella thickness, as well as the etching rate of a single lamella and the etching rate of amorphous material. Hypothetical product build-up on the surface impeding further etching could also have an influence on k and m. This would necessitate the introduction of time-dependant k and m in the equations. Finally, consideration of a non-radial and asymmetric structure for vector **c** near the nucleus could be beneficial for the improvement of the central part of the profile.

Fig. 13 shows the best fit obtained with another material (Polymer A) with the same etching rates ($k = 0.4$ µm/h and $m = 0.65$ µm/h) as those found in Polymer C. In spite of some discrepancies due to large local defects or large receding/protruding lamellae (especially at the top of the two right bands), a good fit is obtained and a true interband distance value of 3.3 µm is obtained. In this fit, experimental data were first corrected with linear baseline removal to properly align the profile with the fitted data axis. An

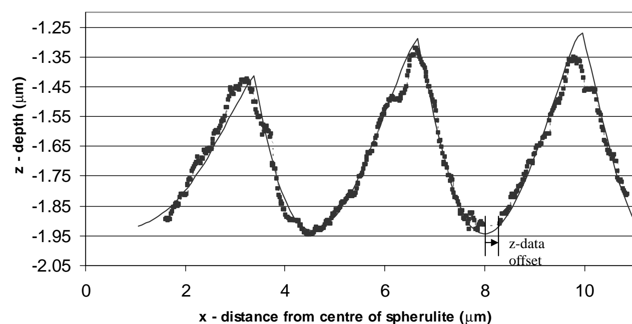

Fig. 13. Etched spherulite vertical cross-section across three bands for Polymer A: experimental AFM data as symbols, compared with the best fit (plain line). Best fit was obtained with the following parameters, $d = 3.3$ µm, $a = -0.85$ µm, $k = 0.4$ µm/h, $m = 0.65$ µm/h, $dt = 0.003$ h, x-interval $= d/100$ µm, with a 5-point Savitsky-Golay smoothing every 100 iterations. The annotation 'x data offset' indicates that the experimental data has been segmented at that abscissa and the right segment slightly shifted horizontally by 0.32 µm. A linear baseline correction was also applied to the experimental data.

Table 2
True interband distance obtained for Polymers A, C and D, using the 'extrapolation method' and with actual model fit data

Reference	Polymer A	Polymer C	Polymer D
True Interband distance (µm) (extrapolation)[a]	3.0 ± 0.3	1.6 ± 0.1	1.9 ± 0.1
True Interband distance (µm) (model fit)	3.3	2.05	2.3
% difference	+ 10%	+ 28%	+ 21%

[a] Method based on the extrapolation of apparent interband distance, published elsewhere [25].

abscissa shift has also been used for the data situated at $x > 8$ μm to properly align the profiles along the whole x-axis. This correction is justified by the observation of irregularities in the images that we may attribute to either defects or a non-ideal spherulite. Interestingly, it can be noted that the fits of Polymer A seem much better at the band minima (in the valleys) than for Polymer C, but the reasons for this have to be explored further. In this respect, the problem of the convolution of the AFM tip with the surface profile, (a well-known AFM artefact) should be explored.

For Polymer D, fits (achieved with the same etching rates) lead to a 2.3 μm interband distance. Table 2 enables us to compare the results for the three materials with the values obtained in the previous work using an extrapolation method based on a formula translating the dependance of the apparent band period to the square root of the band number [25]. We observe that the d values obtained with the present model are always higher than the ones obtained with the extrapolation method and the origin of this discrepancy requires clarification.

If simulations of experimental data lead to good estimates of the k and m etching rates in the future, then it might be possible to deduce from them useful physical and structural information, such as crystallinity or lamella thickness, as well as characteristic etching parameters such as the etching speed of a single lamella or the etching speed of amorphous material.

7. Conclusions

We have developed a mathematical model of permanganic etching capable of fitting the surface relief of etched banded spherulites in polyethylene, as measured by AFM. In particular the band asymmetry characterised by an inner slope lower than the outer slope was correctly simulated. This demonstrates that band asymmetry is not material dependent, i.e. molecular weight or other structural parameters. This model could potentially be applied to any semi-crystalline polymer with lamellar crystals organized in both spherulitic and non-spherulitic morphologies. Not only can this model be used to gain a better understanding of the images observed and provide a better characterisation of the polymers' microstructure, but prospectively, it could also help in understanding the etching processes at the molecular level and in estimating the etching parameters of other polymeric materials.

Acknowledgements

We gratefully acknowledge the support and provision of materials from AtoFina Research, Feluy (Belgium) and Solvay Polyolefins Europe (Belgium).

References

[1] Olley RH, Hodge AM, Bassett DC. J Polym Sci, Polym Phys Ed 1979;17:627.
[2] Olley RH, Bassett DC. Polymer 1982;23:1707.
[3] Olley RH, Bassett DC, Blundell DJ. Polymer 1986;27(3):344.
[4] Hsu TC, Geil PH. Polym Commun 1990;31(3):105.
[5] Muellerleile JT, Wilkes GL, York GA. Polym Commun 1991;32(6):176.
[6] Hudson SD, Lovinger AJ. Polymer 1993;34(6):1123.
[7] Shabana HM, Guo W, Olley RH, Bassett DC. Polymer 1993;34(6):1313.
[8] Vaughan AS. J Mater Sci 1993;28(7):1805.
[9] Palmer RP, Cobbold AJ. Makromol Chem 1964;74:174.
[10] Keller A, Sawada S. Makromol Chem 1964;74:190.
[11] Kanig G. Kolloid-Z u Z Polymere 1973;251:782.
[12] Kanig G. Colloid Polym Sci 1975;57:176.
[13] Naylor KL, Phillips PJ. J Polym Sci, Part B: Polym Phys 1983;21(10):2011.
[14] Freedman AM, Bassett DC, Vaughan AS, Olley RH. Polymer 1986;27(8):1163.
[15] Keller A. Nature 1952;169:913.
[16] Point J-J. Bull Acad R Belgi 1953;39:435.
[17] Keller A. J Polym Sci 1955;17:291.
[18] Point J-J. Bull Acad R Belgi 1955;41:974 (see also p. 982).
[19] Keith HD, Padden Jr. FJ. J Polym Sci 1959;39:101 (see also p. 12).
[20] Keller A. J Polym Sci 1959;39:151.
[21] Price FP. J Polym Sci 1959;39:139.
[22] Hedges ES, Lisengang; Chapman and Hall publishers, London, 1932.
[23] Janimak JJ, Stevens GC. Polymer 2000;41(11):4233.
[24] Shahin MM, Olley RH, Blissett MJ. J Polym Sci, Part B: Polym Phys 1999;37(16):2279.
[25] Janimak JJ, Markey L, Stevens GC. Polymer 2001:1 (in press).
[26] Magonov SN, Reneker DH. Ann Rev Mater Sci 1997;27:175.
[27] Hobbs JK, McMaster TJ, Miles MJ, Barham PJ. Polymer 1998;39(12):2437.
[28] Pearce R, Vancso GJ. J Polym Sci Part B: Polym Phys 1998;36(14):2643.
[29] Pearce R, Vancso GJ. Polymer 1998;39(5):1237.
[30] Pearce R, Vancso GJ. Macromolecules 1997;30(19):5843.
[31] Savitzky A, Golay MJE. Anal Chem 1964;36:1627.
[32] Steiner J, Termonia Y, Deltour J. Anal Chem 1972;44(11):1906.
[33] Madden HH. Anal Chem 1978;50(9):1383.